Magmatic erosion of high-temperature-melting cumulates in the Bushveld Complex by chemical dissolution

Latypov, Rais M.

2022-08

Latypov , R M , Heinonen , J S & Chistyakova , S Y 2022 , ' Magmatic erosion of high-temperature-melting cumulates in the Bushveld Complex by chemical dissolution ' , Geosystems and Geoenvironment , vol. 1 , no. 3 , 100077 . https://doi.org/10.1016/j.geogeo.2022.100077

http://hdl.handle.net/10138/344378
https://doi.org/10.1016/j.geogeo.2022.100077

Geosystems and Geoenvironment 1 (2022) 100077

Contents lists available at ScienceDirect

Geosystems and Geoenvironment

journal homepage: www.elsevier.com/locate/geogeo

Magmatic erosion of high-temperature-melting cumulates in the Bushveld Complex by chemical dissolution

Rais M. Latypov[a,*], Jussi S. Heinonen[b], Sofia Yu. Chistyakova[a]

[a] School of Geosciences, University of the Witwatersrand, South Africa
[b] Department of Geosciences and Geography, University of Helsinki, Finland

ARTICLE INFO

Article history:
Received 29 November 2021
Revised 14 March 2022
Accepted 9 May 2022

Keywords:
Magmatic erosion
Chemical dissolution
Monomineralic cumulates
Replenishing melts
Melt superheating
Bushveld complex

ABSTRACT

The Bushveld Complex in South Africa shows spectacular examples of regional and local magmatic erosion of the floor cumulates by new melt batches that replenished the evolving magma chamber. Field observations indicate that, at some stratigraphic levels, at least, 15–20 m of pre-existing floor cumulates, often nearly monomineralic in composition (e.g., anorthosite or orthopyroxenite) were completely removed on a regional scale. What was the major agent of this erosion – (partial) melting or dissolution of the floor cumulates – remains poorly understood. Thermal melting appears to be a poor candidate because normal basaltic melts (~1220–1260°C) cannot heat up the cumulates up to their melting temperature (~1400–1500°C). We explored, therefore, the possibility of dissolution of these high-temperature-melting cumulates by slightly superheated (15°C above the liquidus) basaltic-andesitic melts that recharged the chamber and spread out laterally along its floor as basal flows. This was done using a freely available thermodynamic tool for phase equilibria modeling of open magmatic systems – the Magma Chamber Simulator. Our thermodynamic modeling shows that the superheated melts can digest up to 4.5–8.0 wt% of the bulk floor cumulates without inducing crystallization of the melts, despite them being much colder than the liquidus temperatures of these cumulates. This is equivalent to regional erosion of 15–24 m of the floor cumulates, given a basal melt layer of about 350 m thick. We conclude that the regional erosion of the high-temperature-melting floor cumulates in the Bushveld chamber has been mostly controlled by their chemical dissolution by replenishing superheated melts.

1. Introduction

One of the most remarkable features of the Bushveld Complex in South Africa (Fig. 1a) – the largest basaltic intrusive complex in Earth's crust (Eales and Cawthorn, 1996; Kruger, 2005; Cawthorn, 2015; Latypov et al., 2022) – is abundant field evidence for intensive removal of the pre-existing cumulates from the instantaneous floor of the magma chamber. The removal is evident at nearly all stratigraphic levels of the complex but is particularly well developed at the level of the Merensky Reef (MR) and UG2 chromitite (Schmidt, 1952; Irvine et al., 1983; Viljoen and Hieber, 1986; Viljoen et al., 1986; Campbell, 1986; Eales et al., 1988; Boudreau, 1992, 2019; Viljoen, 1999; Hornsey, 2004; Van der Merwe and Cawthorn, 2005; Latypov et al., 2015; Mukherjee et al., 2017; Chistyakova et al., 2019a, 2019b) which are mined for platinum group elements (Eales and Cawthorn, 1996; Naldrett et al., 2012; Cawthorn, 2015). The removal at these levels is seen on both the regional scale, where, at least, 10–20 m of cumulates varying in composition from anorthosites to orthopyroxenites appear to have been eliminated (Fig. 1b) and, on a local scale, where in nearly circular excavations, generally known as potholes, footwall cumulates have been eliminated to depths of a few meters to several dozens of meters (Figs. 2 and 3). Although there are concepts that deny the removal of pre-existing cumulates by attributing the field observations to non-deposition of crystals (Ballhaus, 1988), slumping (Leeb-Du Toit, 1986; Hahn and Ovendale, 1994; Carr et al., 1994, 1999) or step-and-stair-type intrusion of syn-magmatic sills (Mitchell et al., 2019b), there seems to be a consensus among most researchers that the missing floor rocks have been eroded away mechanically and/or thermochemically (Schmidt, 1952; Irvine et al., 1983; Campbell, 1986; Eales et al., 1988; Boudreau, 1992, 2019; Viring and Cowell, 1999; Lomberg et al., 1999; Viljoen, 1999; Hornsey, 2004; Smith et al., 2004; Kruger, 2005; Smith and Basson, 2006; Roberts et al., 2007; Maier et al., 2013; Latypov et al., 2015, 2017c, 2017b, 2019; Pebane and Latypov, 2017; Hunt et al., 2018). This magmatic ero-

* Corresponding author.
E-mail address: rais.latypov@wits.ac.za (R.M. Latypov).

https://doi.org/10.1016/j.geogeo.2022.100077

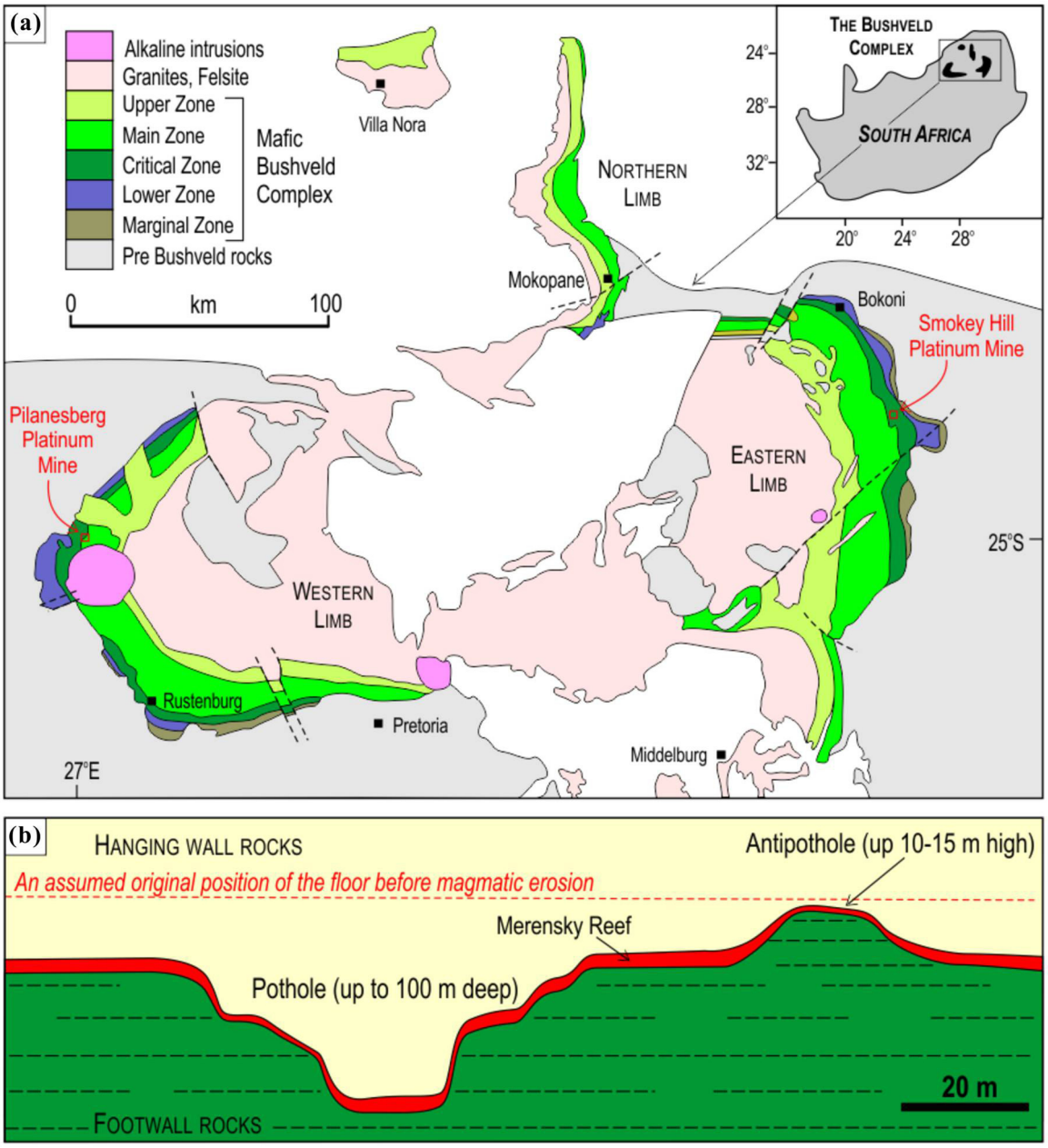

Fig. 1. Geological map and magmatic erosion of floor cumulates in the Bushveld Igneous Complex, South Africa. (a) Location and schematic geological map of the Bushveld Complex (Rustenburg Layered Suite) indicating the location of two mines where most observations reported in this study were made (modified from Latypov et al., 2015). (b) Generalized stratigraphic section illustrating the transgressive relationship of the Merensky Reef (MR) to its footwall. The MR (shown out of scale) overlies relatively planar sections of the temporary floor that have experienced rather uniform erosion, covers near-circular depressions (potholes) that are produced by localized erosion of the floor and drapes over mounds (antipotholes) representing parts of the floor that resisted erosion. The height of antipotholes suggests that, at least, 15–20 m of cumulates could have been eroded away on a regional scale in the Bushveld Complex prior to deposition of the MR. Similar degree of erosion of the floor cumulates has been documented at the level of the UG2 chromitite of the Bushveld Complex (Latypov et al., 2017b). This figure is modified from Latypov et al. (2015).

sion of the pre-existing floor cumulates was commonly attributed to new magma pulses that replenished the evolving chamber (Irvine et al., 1983; Campbell, 1986; Eales et al., 1988; Viring and Cowell, 1999; Lomberg et al., 1999; Viljoen, 1999; Hornsey, 2004; Roberts et al., 2007) – a concept that finds a strong support from a large body of recent field, textural and chemical observations from various parts of the Bushveld Complex (Latypov et al., 2015, 2017a, 2017c, 2017b, 2018a, 2019, 2020a; Mukherjee et al., 2017; Pebane and Latypov, 2017; Hunt et al., 2018; Chistyakova et al., 2019b, 2019a, 2021; Kruger and Latypov, 2020, 2021; Hasch and Latypov, 2021; Latypov et al., 2022). Despite these observational findings, the exact mechanism of the magmatic erosion – e.g., mechanical, thermal or chemical – remains controversial (see discussion in Latypov et al., 2017a, 2019). Although mechanical disruption of cumulates by crystal-rich slurries has been likely involved in the erosional process (e.g., Maier et al., 2016; Latypov et al., 2017b), this process is unlikely to be a major agent because the amount of xenoliths is small to non-existent in most places (e.g., Latypov et al., 2015, 2017a, 2017c, 2019). Therefore, it seems more likely that the missing floor cumulates in the Bushveld Complex have either been melted thermally or dissolved chemically by melts replenishing the evolving magma chamber. Both processes have some inherent limitations which are in the focus of our current study. A key finding of our thermodynamic analysis

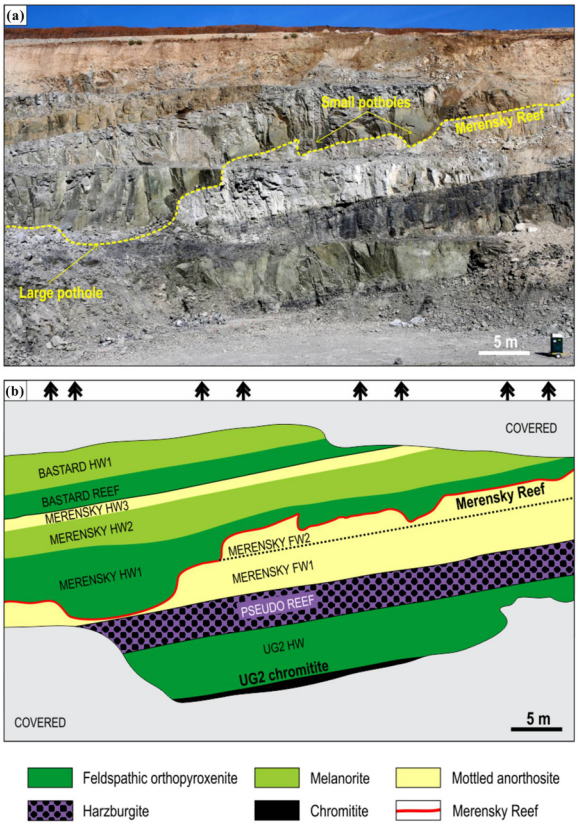

Fig. 2. Magmatic erosion of floor cumulates in the Bushveld Complex. Photograph (a) and sketch (b) of a cross-section through the part of the Upper Critical Zone in the open pit of the Pilanesberg Platinum Mine, Western Bushveld Complex. Note one large pothole developed in the mottled anorthosite underlying the Merensky Reef. Location of the mine on a schematic map of the Bushveld Complex is shown in Fig. 1. This figure is modified from Latypov et al. (2019).

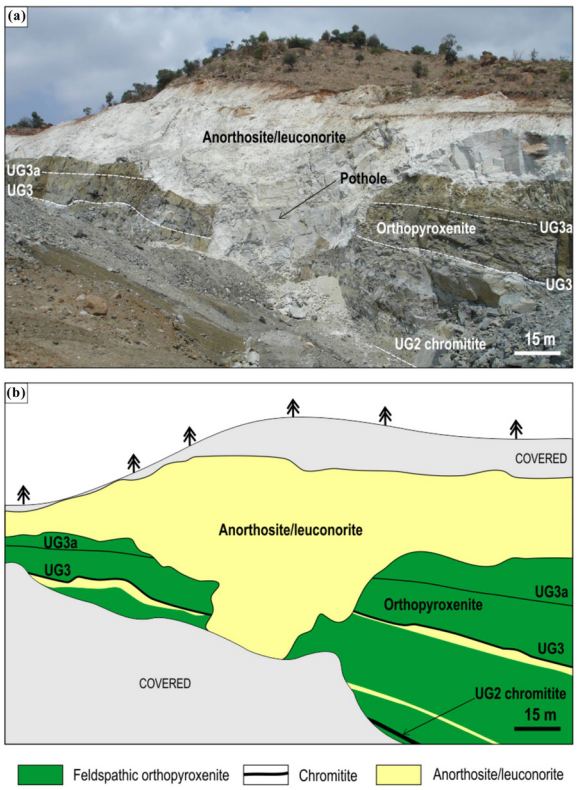

Fig. 3. Magmatic erosion of floor cumulates in the Bushveld Complex. Photograph (a) and sketch (b) showing a large anorthosite pothole that transgresses mostly orthopyroxenitic footwall rocks of the Upper Critical Zone in the open pit of the Smokey Hills mine, Eastern Bushveld Complex. Note one large pothole developed in the mottled anorthosite underlying the Merensky Reef. Location of the mine on a schematic map of the Bushveld Complex is shown in Fig. 1. This figure is modified from Latypov et al. (2020).

based on the Magma Chamber Simulator (MCS) – a new thermodynamic tool for phase equilibria modeling of open magmatic systems (Bohrson et al., 2014, 2020) – is that chemical dissolution is likely the most viable mechanism for the intensive magmatic erosion of the pre-existing floor cumulates in the Bushveld Complex.

2. Geological and petrological background

The 2.05 billion-years-old Bushveld Complex in South Africa (Fig. 1a) occupies an area that most likely exceeds 100,000 km^2 and extends ~450 km East-West and ~350 km North-South (Cawthorn and Walraven, 1998; Naldrett et al., 2012; Cawthorn, 2015; Finn et al., 2015). The complex consists of several parts, the western, eastern and northern limbs being the largest, and is subdivided stratigraphically into five major units – the Marginal, Lower, Critical, Main, and Upper Zones, comprising a total thickness of about 7 to 9 km (Cawthorn, 2015). The Bushveld Complex is widely considered as a typical example of an open-system magma chamber (Kruger, 2005). Apart from the marginal rocks, its four principal zones are attributed to major replenishment events, with numerous smaller magmatic recharges contributing to the formation of these zones. During this process, the magma chamber was incrementally increasing in size by inflation both vertically and laterally (Willemse, 1959; Eales, 2002; Kruger, 2005). All major replenishment events are marked by regionally extensive magmatic disconformities, local unconformities with erosion of previous strata, significant isotopic shifts, and notable changes in whole-rock and mineral compositions (Kruger, 2005). In this study we concentrate our thermodynamic modeling on two reported occurrences of floor cumulate erosion related to the Upper Critical Zone (UCZ) of the Bushveld Complex. These are: (1) the magmatic erosion of anorthosites observed in the open pit of the Pilanesberg Platinum Mine (PPM), North-Western Bushveld Complex (Case 1; Fig. 2; Latypov et al., 2019) and (2) the magmatic erosion of orthopyroxenites observed at the Smokey Hills Mine (SHM), Eastern Bushveld Complex (Case 2; Fig. 3; Latypov et al., 2020a).

In Case 1, the stratigraphic sequence at the PPM open pit from the base upwards consists of five major units including the UG1 Unit, the UG2 Unit, the Pseudo Reef Unit, the Merensky Unit and the Bastard Unit, along with the intervening leuconorite to anorthosite layers (Fig. 2; Viljoen et al., 1986; Mitchell et al., 2019b, 2019a; Latypov et al., 2019). One impressive outcrop of this sequence in the PPM open pit comprises a ~55 m thick continuous and undisturbed section from the UG2 chromitite layer up to Bastard Unit norite (Fig. 2). A layer of mottled anorthosite that underlies the Merensky Unit is of most interest here because it shows one large and two small transgressive potholes filled in by the Merensky Unit orthopyroxenite. The magmatic erosion of the anorthosites results in contrasting morphology of the upper and lower contacts of this layer with the host rocks, with the lower contact being flat and planar whereas the upper contact is highly scalloped and irregular. The irregularities of the upper contact result in notable variations in the anorthosite thickness including its almost complete disappearance at the base of a large pothole (Fig. 2). Despite the intensive potholing of this layer of footwall anorthosite, no deformation/disruption is observed in either the underlying Pseudo Reef Unit or the overlying layers of

the Merensky and Bastard Units. Also, no xenoliths of footwall anorthosite are observed within potholes of the Merensky Unit (Fig. 2; Latypov et al., 2019).

In Case 2, the stratigraphic sequence at the SHM open pit from the base upwards consists of three major units including the UG2 Unit, the UG3 Unit and the Merensky Unit (Fig. 3; Gain, 1985; Maier et al., 2016). One outcrop of this sequence comprises a ~25 m thick section from the UG2 chromitite layer up to mottled anorthosite footwall of the Merensky Unit (Fig. 3) and is remarkable in showing a pothole that cuts down up to a dozen of metres through the underlying stratigraphy. This pothole is filled with the MR footwall layer of anorthosite/leuconorite that overlies a sequence of UG2/UG3/UG3a mafic-ultramafic units. The UG2 unit is composed of a thick chromitite layer overlain by orthopyroxenite with some norites and anorthosite sublayers. The UG3/UG3a units comprise thinner chromitite layers mostly overlain by orthopyroxenite. The pothole cuts through the entire underlying sequence down to the UG2 chromitite. The transgression is well seen from the discordant relationships of UG3/UG3a chromitite and anorthosite with the sub-vertical margins of the pothole (Fig. 3). In the pothole, the cross-cutting relationships are particularly evident from the occurrence of angular to sub-rounded blocks of footwall rocks within anorthosite/leuconorite, from the highly undulating and scalloped nature of the basal contact of the potholed anorthosites and from the local invasion of thin offshoots of anorthosite from steeply-inclined sidewalls into adjacent footwall orthopyroxenite (Maier et al., 2016; Latypov et al., 2020a, 2020b).

3. Thermodynamic modeling

3.1. Background

3.1.1. Melting vs. dissolution in igneous systems

The distinction between a substance melting and dissolution is not always clear in literature. In terms of thermodynamics, the issue is semantic. For example, does an ice cube melt or dissolve in a glass of water at room temperature (20°C)? It could be argued that the process is melting, since there really is no solvent or solute in a system composed of a single component (H_2O). Thermodynamically, it can be stated that an ice cube of a given mass and temperature (and thus of enthalpy) mixes with a given mass and temperature of water; when the mixture equilibrates at the ambient room temperature, the system arrives at a final state of a single-phase liquid. This thermodynamic statement does not differentiate between the two processes, the distinction of which could then be considered semantic.

A look into a two-component two-phase system gives more insight into the subject. A useful analogue is pouring a spoonful of table salt (halite, NaCl) in a glass of water at room temperature. Melting point of pure halite is 801°C at atmospheric pressure (Robie and Waldbaum, 1968) Nevertheless, if water is not saturated in halite, halite disintegrates, and a homogeneous solution is generated. Therefore, it could be argued that halite must have dissolved in water. A simple example relevant to magmas, is illustrated for the binary system An-Di (Fig. 4a; Bowen, 1915; Yoder, 1976). Although anorthite may crystallize in this system from melt X at 1300°C, the cumulates composed of the anorthite (i.e., anorthosite), if isolated from the system, may melt only at 1553°C (at point X'). This is 253°C higher than the temperature at which anorthite originally crystallized. However, if these anorthite crystals are then put into a melt that is undersaturated in anorthite (for example, at point Z), they start dissolving regardless of the relatively low temperature of the melt.

Following Kerr (1995), we treat melting and dissolution in an igneous system in this study as follows. Melting takes place when the temperature of a crystal (or a rock) is above its melting temperature (or solidus temperature). This requires only diffusion of heat, although assimilation of the formed melt by another (resident) melt also requires mass to be transported. Dissolution results from a chemical disequilibrium between a crystal and melt and may occur even when they are at the same temperature or if the crystal has a higher melting temperature than that of the melt. For the case of a magma chamber, this means that dissolution happens directly at the melt-solid interface whereas thermal melting may also take place beyond this interface in the country rock. Although in the case of dissolution only diffusion of mass through the crystal-melt interface is required, in magmatic systems thermal disequilibrium and thus diffusion of heat almost always take place. We emphasize again that purely thermodynamic models, such as MCS, do not consider kinetic factors, such as thermal or chemical diffusion.

The binary example in Fig. 4a stresses the fundamental difference between parental liquids and cumulates with regards to their liquidus and solidus temperatures (e.g., Morse, 1980). In contrast to simple melt-crystal systems or other such binary analogues given above and as modeled by Kerr (1995), however, magmas are usually composed of plethora of chemical components, and can simultaneously host various different solid, liquid, and gaseous phases. Instead of a single crystallization or melting temperature, the difference between the solidus and liquidus temperatures of rocks and magmas may thus be hundreds of degrees °C (Fig. 4b, c).

Textural, experimental and modeling evidence indicate that, under favorable conditions, differentiating magmas are able to digest significant amounts of solid phases – having high melting temperatures – that are not saturated in them (e.g., Müller et al., 2005; Mungall, 2007; Iacono-Marziano et al., 2017). To evaluate the relative roles of dissolution and melting in assimilating magmatic systems by modeling, a thorough treatment of the associated energetics and phase equilibria is required.

3.1.2. The utilization of the Magma Chamber Simulator

The issue of melting versus dissolution in the formation of the regional and local erosional features of the Bushveld Complex (Figs. 1-3) are examined here using the Magma Chamber Simulator (MCS) – a thermodynamic model that can be used to compute the phase, thermal, and compositional evolution of a multiphase – multicomponent system of a fractionally crystallizing resident body of magma, linked wallrock, and recharge reservoirs (Bohrson et al., 2014, 2020). The thermodynamic engine of the MCS is built on MELTS-family of algorithms (either rhyolite-MELTS or pMELTS; Ghiorso et al., 2002; Gualda et al., 2012; Ghiorso and Gualda, 2015).

Assimilation and concurrent crystallization can be modeled in two different ways in the MCS (Fig. 5). The first is progressive assimilation of wallrock anatectic melts – fractional crystallization (MCS-AFC), where the wallrock melts are formed by enthalpy released by sensible and latent heat derived from the cooling and crystallization of magma. A wallrock melt formed above a user-defined percolation threshold value (fmZero), is mixed and homogenized with the resident magma. MCS-AFC modeling can be used to estimate the effective maximum limit of wallrock assimilation by (partial) melting (Heinonen et al., 2021).

In bulk assimilation of stoped blocks-fractional crystallization (MCS-SFC), a user-input mass of stoped wallrock is forced to homogenize and equilibrate with the resident melt during one simulation step (Fig. 5). MCS-SFC does not consider the actual process of homogenization, or the scale of it (e.g., whether the block mass is composed of a single block or a collection of infinitesimally small blocks), but provides thermodynamic consequences of forced homogenization and thus a valuable comparison to MCS-AFC modeling results (Bohrson et al., 2020; Heinonen et al., 2021).

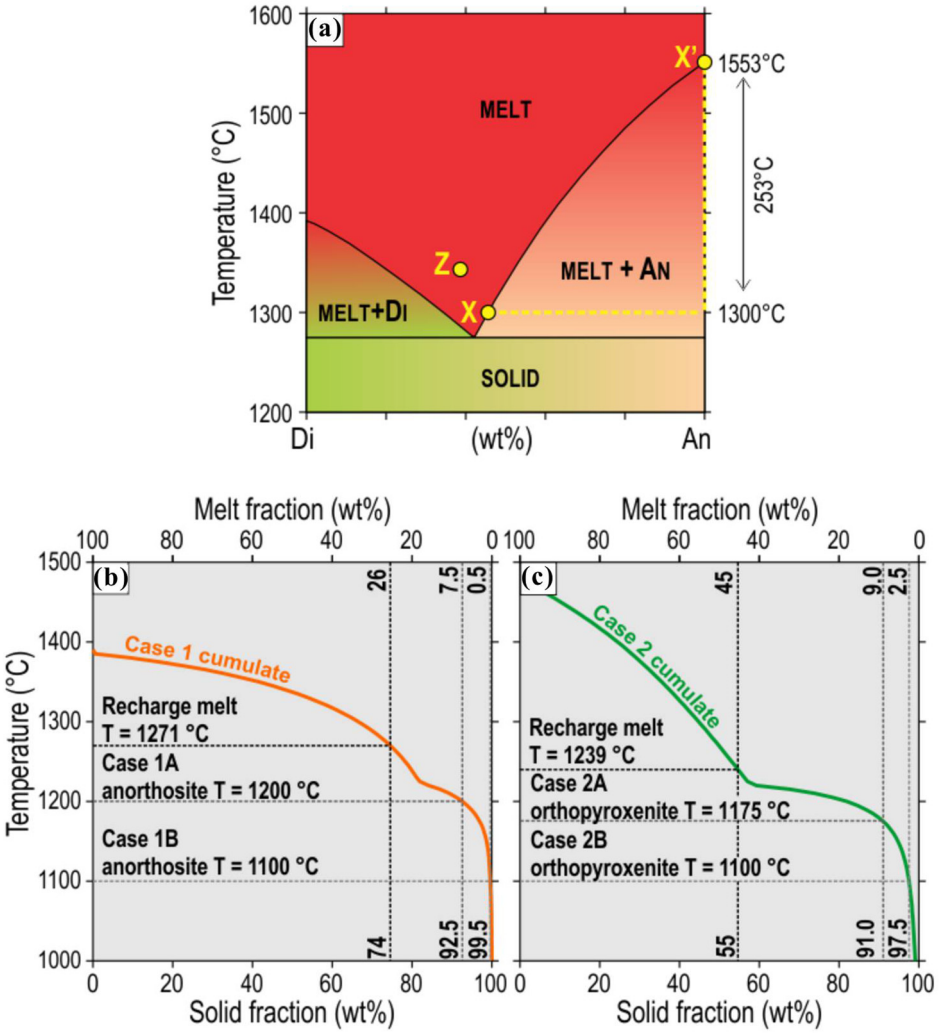

Fig. 4. Liquidus phase diagram of the binary anorthite-diopside (An-Di) system at 1 atm (a; modified from Presnall et al., 1978) and temperature versus solid/melt fraction relationships for the floor cumulates of Case 1 (b) and Case 2 (c). The phase diagram (a) illustrates that melting of anorthite cumulates (point X') isolated from the system would require a temperature of 253°C higher than the temperature at which anorthite originally formed in the mixture (point X). Yet, anorthite would begin dissolving if introduced in a melt at point Z. The temperature versus melt fraction diagrams (b and c) indicate the relative amounts of melt and solid in the floor cumulates at 1) case-specific recharge melt temperatures, 2) initial cumulate temperature of 1200°C (Case 1A) and 1175°C (Case 2A), and 3) initial cumulate temperature of 1100°C (Cases 1B and 2B). Note that the curves do not take account phase changes caused by assimilation of the formed partial melts in the floor cumulate, which takes place in the MCS-AFC models. These curves are shown just to highlight the state of the bulk cumulate at relevant model temperatures. See Supplementary Data and Table 3 for more details.

In both models (MCS-AFC and MCS-SFC), the contaminated resident magma system – and residual wallrock in the former – comes to a new equilibrium state at a new temperature (Fig. 5). Crystallization and/or separation of a fluid phase can occur due to the assimilation events and the resident melt composition records the resulting compositional changes. If a stoping event does not result in crystallization in the resident magma, the magma remains undersaturated in solid phases and is thus able to completely digest the stoped block, regardless of whether this would occur by partial melting or dissolution or both.

For a more thorough explanation of how the software and MCS-AFC and MCS-SFC work, the reader is referred to Bohrson et al. (2014, 2020).

3.2. Modeling input and procedure

The erosion (assimilation) of anorthosites at the PPM (Case 1) and orthopyroxenites at the SHM (Case 2) by recharge melts of basaltic-andesitic composition (Latypov et al., 2018b, 2020a) were modeled by both MCS-AFC and MCS-SFC and using rhyolite-MELTS v.1.2.0 as the thermodynamic engine (Gualda et al., 2012; Ghiorso and Gualda, 2015; see http://melts.ofm-research.org/MELTS-decision-tree.html). In the MCS-SFC simulations, we tested the maximum mass of a floor cumulate block which the melt could assimilate without inducing crystallization. These results were then compared to those of the MCS-AFC simulations, in which the equivalent mass of floor cumulate was heated and partially melted by the parental melt. In addition to MCS, we used stand-alone rhyolite-MELTS v.1.2.0 to study the phase equilibria and melt fraction of the floor cumulates (in isolation from the magma) at varying temperature (see Fig. 4b, c).

The compositional parameters are based on earlier work on the relevant melt and cumulate compositions of both cases and are listed in Table 1. Note that the replenishing melts that reacted with the floor cumulates are defined as the parental melts in the MCS model setting. This is because we are interested in starting the models at the exact moment of when the reactions with the replenishing melt begin. The parental melt for Case 1 is a basaltic-andesitic melt composition reported in Latypov et al. (2018b). The associated floor cumulate, i.e., wallrock, is average of anorthosite

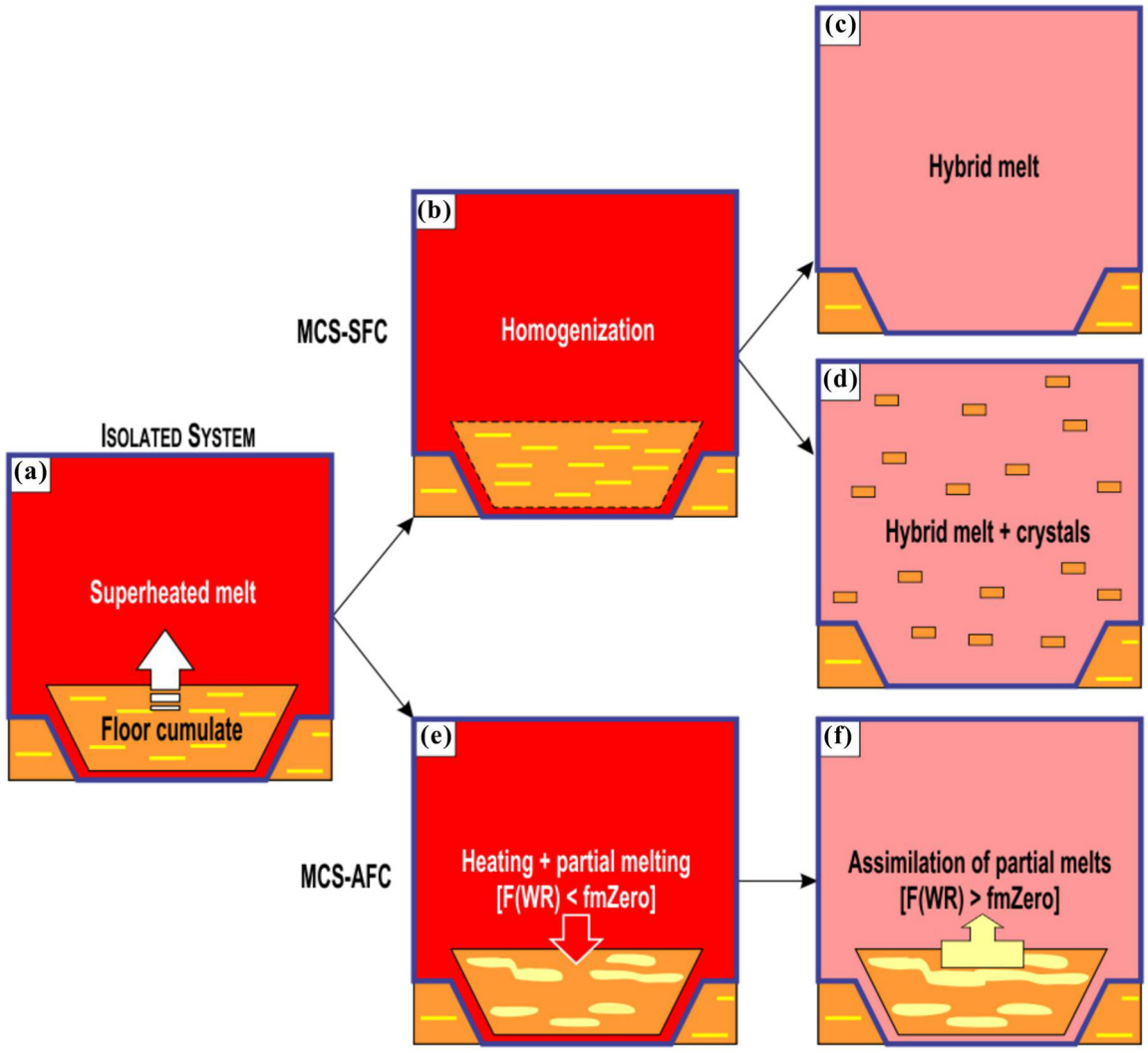

Fig. 5. A schematic presentation of the thermodynamic modeling and the differences between the MCS-SFC and MCS-AFC simulations. We consider an isolated system (indicated by a blue line) where a block of floor cumulate, here consisting of two mineral phases, is introduced and becomes part of an isolated system that comprises the block and superheated melt (a). The changing color of the resident melt in (c), (d), and (f) indicates its differentiation to more evolved composition. In MCS-SFC, the block is homogenized with the resident melt within one simulation step (b). We focus our attention on two possible outcomes of this forced and thorough reaction: after homogenization, the system may remain undersaturated in solid phases (c) or crystals may form in the resident melt (d). In the latter case, the wholesale assimilation of the block could be considered improbable, especially if the crystals are of the same phase than in the floor cumulate. In MCS-AFC, the superheated melt heats the wallrock block (e). If its solidus temperature is surpassed, it starts to partially melt as illustrated here in the vicinity of the original phase contacts. When the percolation threshold (fmZero) of the cumulate block has been surpassed, the partial melts are introduced in the resident melt (f). Note that in the case of superheated melt, latent heat of crystallization is not required in order for the floor cumulate to partially melt and get assimilated in the MCS-AFC models (see Supplementary Data). Since the heat released by the magma would also be conducted in the remaining cumulates (here illustrated outside of the isolated system) and not only in the separated block in nature, the degree of melting of the given block as suggested by the MCS-AFC modeling could be considered as absolute maximum. Abbreviations: F = degree of melting, WR = wallrock.

compositions reported by Chistyakova et al. (2019a). The parental melt for Case 2 is also a basaltic-andesitic melt, but of slightly different composition reported in Latypov et al. (2020). The associated floor cumulate, i.e., wallrock, is average of orthopyroxenite compositions reported by Chistyakova et al. (2019a). The oxidation state of the floor cumulates is unknown, but Fe^{3+} is assumed to behave incompatibly during fractionation, however, and thus a low value of Fe^{3+}/Fe^{tot} (0.05) has been used for the cumulates in the models. The choice of this value is expected to have no meaningful effect on the results of the modeling (see Heinonen et al., 2019). For the parental melts, Fe_2O_3 and FeO contents were given in the original sources.

Studies have shown that for chemical dissolution to work in layered intrusions, the replenishing melt (solvent) must be in chemical disequilibrium with the floor cumulates (solute) and it needs to be somewhat superheated relative to its liquidus temperature (e.g., Irvine et al., 1983; Campbell, 1986; Latypov et al., 2017a, 2017c). Superheating of the replenishing melt is required because melts at liquidus temperature may start crystallizing soon after their arrival into the chamber and will therefore form a new layer of cumulates covering the pre-existing floor cumulates and thus inhibiting the dissolution process. The superheating may result from the rapid ascent of a large volume of hot melt from the deep-seated reservoir so that little cooling happened against the cold crustal rocks (e.g., Latypov et al., 2018b, 2020a) and/or mixing of new magma with the resident melt upon entry into the chamber (Irvine et al., 1983; Campbell, 1986; Latypov et al., 2015). During ascent the melt superheating arises owing to the difference in slope between the adiabatic gradient and the liquidus and its degree can be up to 90°C for magma ascending from a storage region located at a depth corresponding to a pressure difference of about 10 kbar (an assumed position of a Bushveld staging

Table 1
Selected input for the MCS modeling.

	Case 1 Parental melt	Floor cumulate	Case 2 Parental melt	Floor cumulate
Type	basaltic andesite	anorthosite	basaltic andesite	orthopyroxenite
SiO_2 (wt%)	55.05	49.34	54.16	52.93
TiO_2	0.11	0.07	0.13	0.22
Al_2O_3	17.41	30.10	20.00	8.96
Fe_2O_3	0.90	0.08	0.63	0.58
Cr_2O_3	0.10	0.03	0.00	0.32
FeO	7.91	1.29	4.89	9.98
MnO	0.00	0.03	0.00	0.19
MgO	6.69	1.49	7.00	20.04
NiO	0.00	0.00	0.00	0.00
CoO	0.00	0.00	0.00	0.00
CaO	9.83	14.92	10.00	5.79
Na_2O	1.44	2.46	2.50	0.79
K_2O	0.11	0.19	0.14	0.18
P_2O_5	0.00	0.00	0.00	0.00
H_2O	0.45	0.00	0.55	0.00
CO_2	0.00	0.00	0.00	0.00
Liquidus T (°C)	1256	1390	1224	1485
Initial T (°C)	1271	1100 or 1200	1239	1100 or 1175

Sources: see Section 3.2.

chamber at the Moho; Latypov et al., 2020a). In reality, some cooling of rising melts still inevitably occurs so that upon arrival into a shallow-level Bushveld chamber they may be much less superheated. The exact degree of superheating is not possible to predict but 5–15°C above liquidus was considered as a reasonable estimation (Latypov et al., 2017b, 2017c, 2020a) .

The initial parental melt mass in MCS is always 100 units. The superheating of the parental melt in our modeling is taken at 15°C above liquidus. The MCS does not allow parental melt to be in a superheated state, however: if the initial temperature is higher than the respective liquidus temperature, MCS automatically decreases the temperature to the liquidus temperature upon model initiation. We circumvented this internal limitation by introducing a second batch of superheated parental melt (100 units) as early as possible, i.e., after the first temperature decrement and minimal amount (<0.5 wt%) of crystallization. The temperature of the second batch was iterated so that the magma chamber had a melt mass of ~200 units and temperature ~15°C above liquidus of the parental melt composition before any assimilation took place. In addition to the superliquidus models, we also ran some secondary models using the liquidus temperature as the initial temperature. These simulations were performed only to test whether bulk digestion of a small cumulate block is possible without inducing crystallization in the parental melt at its initial liquidus.

The temperature decrement step in the models was set to 1°C. Within this step, and if subsolidus, the system crystallizes in equilibrium after which the formed crystals ± fluids are fractionated away from the system. A low value was chosen because we wanted to minimize the amount of system cooling and crystallization preceding any other events in the modeling. Using a larger decrement step, like 2 or 5°C, would not be expected to have any other major effect on the outcomes of the models. The pressure was set to 200 MPa (2 kbar) which corresponds to the depth at which cumulate reaction with magma took place (e.g., Latypov et al., 2020a).

In the MCS-SFC simulations, the stoped floor cumulate block was introduced in the resident magma as early as possible (after 1°C decrement following the superliquidus treatment of the parental melt as described above). The mass of the stoped block was iterated so that it was the maximum amount allowed in the simulation without inducing crystallization in the resident melt after the following temperature decrement step. In the MCS-AFC simulations, the melt percolation threshold value of the wallrock (fmZero) was selected to be 0.1, which is relevant for non-

Table 2
Equilibrium phase states of the floor cumulates at the model initial temperatures.

Case 1 anorthosite	melt	ol	opx	cpx	plag	spl
wt% at 1200°C	7.47	–	–	4.69	87.76	0.08
wt% at 1100°C	0.47	0.12	–	7.9	91.4	0.11
Case 2 orthopyroxenite						
	melt	ol	opx	cpx	plag	spl
wt% at 1175°C	8.99	0.47	41.01	31.72	16.9	0.91
wt% at 1100°C	2.51	1.07	67.77	5.75	21.98	0.92

Abbreviations: ol = olivine, opx = orthopyroxene, cpx = clinopyroxene, plag = plagioclase, spl = spinel. Note that this information is not directly minable from the MCS output, but was gathered from EQ runs using standalone rhyolite-MELTS v.1.2.0 (Gualda et al., 2012; Ghiorso and Gualda, 2015).

texturally equilibrated rocks (Cheadle et al., 2004) such as cumulates. This means that before any assimilation of the wallrock partial melt takes place, the floor cumulate must be 10 wt% molten. The mass of the wallrock was varied according to the results of the MCS-SFC simulations and is discussed in the results section.

We varied the initial temperatures of the floor cumulates in MCS-AFC and MCS-SFC simulations and used end-member values of 1200°C (Case 1A) and 1100°C (Case 1B) for Case 1 and 1175°C (Case 2A) and 1100°C (Case 2B) for Case 2 (Fig. 4b, c). This range is relevant to the modeled environment, where the floor cumulates were unlikely to have been fully crystalline before the emplacement of the replenishment magma. The lower maximum initial temperature for Case 2 is because at temperatures higher than 1175°C, the melt fraction of the orthopyroxenite cumulate was above the percolation threshold of 10 wt% melt (Fig. 4c).

For a more detailed description of the modeling appended with screenshots from the MCS files, see Supplementary Data.

3.3. Results of the MCS modeling

The results of our MCS and rhyolite-MELTS modeling are presented in Tables 2 and 3 and in Fig. 6. Full output in the form of the primary MCS-generated Microsoft Excel files is included in the Supplementary Data.

Table 2 illustrates the strength of using multiphase-multicomponent tools in thermodynamic modeling of igneous systems. Although the floor cumulates are probably not in internal equilibrium in nature like they are in the models, it is clear

Table 3
Results of the MCS modeling.

Model # MCS-SFC results	PM T_{liq}; T_{ini} (°C)	WR T_{liq}; T_{ini} (°C)	WR F_{ini} (wt%)	WR m_{ini} / PM m_{ini} (wt%)	A_{MAX} / PM m_{ini} (wt%)	A_{MAX} / WR m_{ini} (wt%)	ρ after A_{MAX} (kg/m^3)
Case 1: Pilanesburg mine anorthosites							PM_{ini}: 2614
1A	1256; 1271	1390; 1200	7.5	4.5	**4.5**	**100.0**	2614
1B	1256; 1271	1390; 1100	0.5	3.5	**3.5**	**100.0**	2615
Case 2: Smokey Hills mine orthopyroxenites							PM_{ini}: 2576
2A	1224; 1239	1485; 1175	9.0	8.0	**8.0**	**100.0**	2591
2B	1224; 1239	1485; 1100	2.5	7.0	**7.0**	**100.0**	2590
MCS-AFC results							
Case 1: Pilanesburg mine anorthosites							PM_{ini}: 2614
1A	1256; 1271	1390; 1200	7.5	4.5	**0.5**	**11.4**	2614
1B	1256; 1271	1390; 1100	0.5	3.5	**0.5**	**12.9**	2615
Case 2: Smokey Hills mine orthopyroxenites							PM_{ini}: 2576
2A	1224; 1239	1485; 1175	9.0	8.0	**2.4**	**30.5**	2579
2B	1224; 1239	1485; 1100	2.5	7.0	**1.6**	**23.0**	2579

Abbreviations: PM = parental melt, WR = wallrock, T = temperature, F = degree of interstitial melt, m = mass, A = assimilation, liq = liquidus, ini = initial, MAX = maximum.

that neither of the floor cumulates are purely monomineralic at 1100–1200°C but are composed of several solid phases. This is because our modeling is based on actual measured compositions of the floor cumulates and not idealized compositions of pure solid phases like in simple models of binary systems (cf. Fig. 4a; see Section 3.1.1). Mixtures of substances always have lower melting points than pure substances: for example, Case 1 anorthosite with An_{76} plagioclase is 7.5 wt% molten already at 1200°C (at 200 MPa; Table 2; Fig. 4b), although pure anorthite has a melting point of 1553°C (at atmospheric pressure; Fig. 4a).

The first question to answer was that what is the maximum mass of floor cumulates that the superliquidus melts can assimilate without inducing crystallization in the MCS-SFC simulations. Only the final iterated model result is displayed in Table 3 and included in the Supplementary Data. In Case 1, the MCS-SFC simulations suggest that the basaltic-andesitic melt can absorb 3.5–4.5 wt% (relative to the mass of the parental melt) of anorthosite cumulate without inducing crystallization (Fig. 6b). In Case 2, the basaltic-andesitic melt can absorb 7.0–8.0 wt% of orthopyroxenite cumulate without inducing crystallization (Fig. 6d). Such masses are able to explain the scale of magmatic erosion of the floor cumulates in the Bushveld Complex (see next section).

Using the above masses of floor cumulate in the MCS-AFC simulations enables us to study the potential of partial melting in floor cumulate assimilation (Table 3). If subjected to heating and partial melting, the floor cumulate masses that are equal to the masses of the fully digested stoped blocks in the MCS-SFC models can partially melt in amounts of 11–13 wt% (Case 1) and 23–30 wt% (Case 2), which results in degrees of assimilation of only ~0.5 wt% and 1.6–2.4 wt% relative to the parental melt, respectively. Even at the respective superheated recharge melt temperatures, the melt fractions of the floor cumulates would only be 26 and 45 wt%, respectively (Fig. 4b, c). Such degrees of melting would require constant addition of recharge melts to prevent cooling of the system below the superliquidus temperatures of the parental melts. Collectively, the results show that in the case of bulk assimilation, chemical dissolution must dominate over thermal melting as the primary assimilation process in the modeled scenarios – this will be discussed in more detail in the next section.

4. Discussion and implications

Our modeling indicates that a reaction of inflowing superheated melt with pre-existing floor cumulates (anorthosite or orthopyroxenite) results in a mass loss of solidified rocks (Fig. 6). The thermodynamic models do not directly assess whether this loss of mass takes place by partial melting or dissolution or both, but modeling suggests that dissolution must dominate the process of bulk assimilation. The floor cumulate masses that can be absorbed by basaltic-andesitic melts in our MCS-SFC simulations (3.5–4.5 wt% for Case 1 and 7.0–8.0 wt% for Case 2) are more than enough to explain the estimated relative masses of the magma and eroded cumulates based on field observations of the Bushveld Complex. As an illustration, this means that a 350 m thick basal layer of superheated melt would be able to fully digest about 12–15 m and 20–24 m of the high-temperature-melting floor cumulates of anorthositic and orthopyroxenitic composition, respectively (Fig. 6a-d). It is important to note that the amount of interstitial melt in the cumulates at the modelled temperatures (1100–1200 °C) is taken relatively small: 0.5–7.5 wt% in Case 1 and 2.5–9.0 wt% in Case 2. The choice is governed by field and textural data indicating that a mushy zone in the Bushveld Complex and other layered intrusions is, at best, only a few meters thick (Hess, 1960; Irvine et al., 1998; Latypov et al., 2015, 2020b; Holness et al., 2017) and, in some cases, can be even close to zero (Kruger and Latypov, 2020, 2021). In essence, we consider here a case of chemical dissolution of the chamber floor that is nearly completely solid (e.g., Latypov et al., 2020b), as opposed to other extreme where the floor is a partially molten mush with variable proportion of interstitial liquid (Marsh, 1996, 2006, 2013). In the latter case, the degree of assimilation would be expected to be even higher.

Is it really necessary for the replenishing melts to be superheated to be able to dissolve the pre-existing cumulates? The question is quite relevant because the modeling of binary systems shows that the net dissolution of solid phases is actually possible even if the parental melt is initially at its liquidus temperature (see Kerr, 1995; Spera et al., 2016). We tested this by running additional simulations at liquidus T of the parental melts: bulk assimilation of even 0.5 wt% of floor cumulate is not possible in either such case without inducing crystallization (see Supplementary Data). Yet, in the field, textural and chemical evidence indicate that both melt crystallization and dissolution of cumulates in the Bushveld Complex occur at the same place, i.e., at the floor of a magma chamber (Latypov et al., 2015, 2017c, 2017b, 2019; Pebane and Latypov, 2017; Hunt et al., 2018; Chistyakova et al., 2019a; Kruger and Latypov, 2020, 2021). The logic suggests that these two events must be separated in time – e.g., first, to dissolve the floor cumulates by replenishing melt and only then crystallize the new cumulates from this melt (or new one) at the erosional surface of the chamber floor. To have these two processes working at the same time and at the same place is physically impossible (see more discussion of this issue in Latypov et al., 2017a). This means that effective bulk assimilation as observed in the two examined cases (Figs. 2-3) requires the presence of superheated

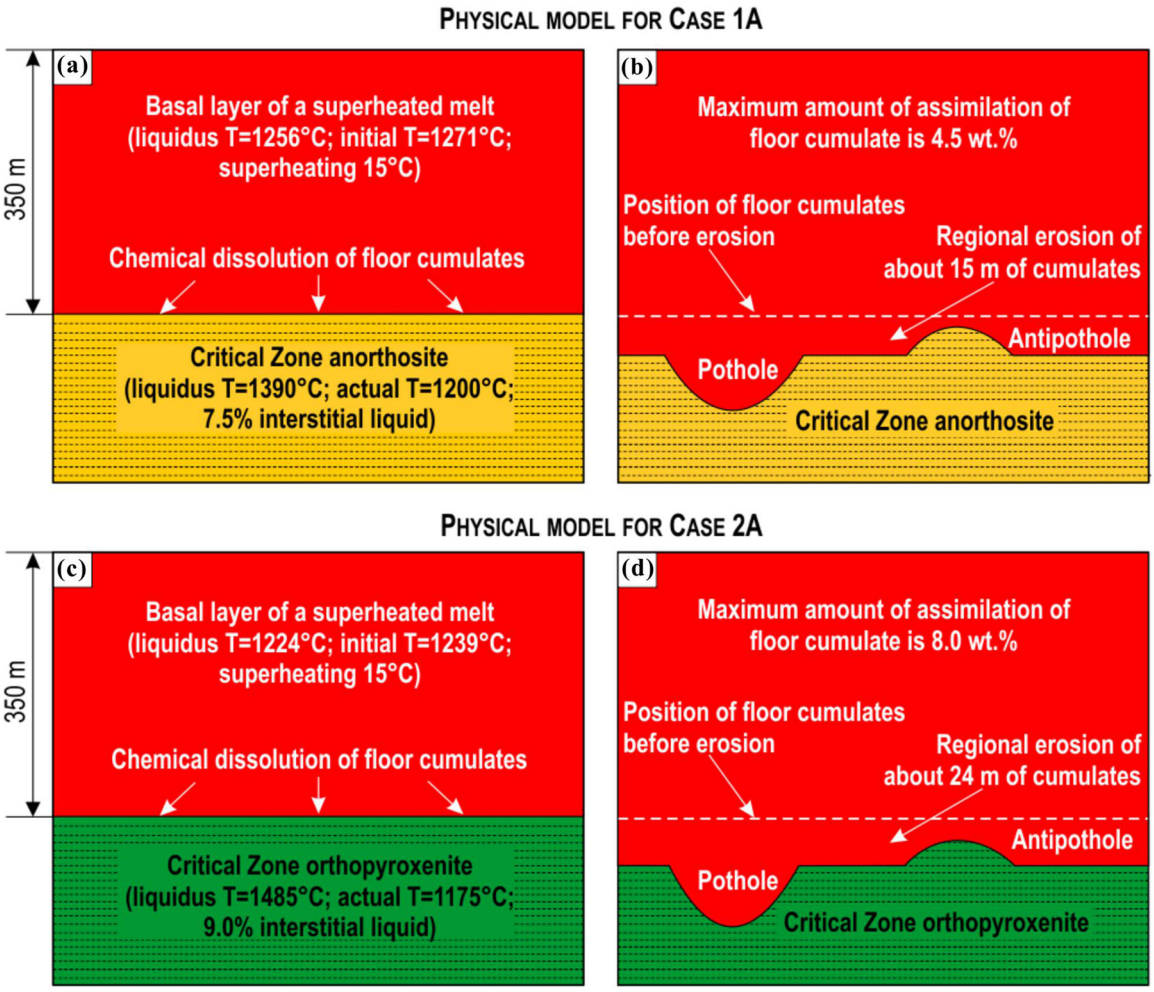

Fig. 6. A model for the maximum erosion of the floor cumulates in the Bushveld Complex observed in Cases 1A and 2A in Table 3. (a and b) A dense superheated melt entered the chamber and spread across the floor of the chamber as a 350 m thick basal layer beneath a resident melt. The superheated melt caused regional erosion of about 15 m thick anorthosites at the temporary floor of the chamber by chemical dissolution, developing in addition potholes and antipotholes within the footwall rocks (shown out of scale). (c and d) A dense superheated melt entered the chamber and spread across the floor of the chamber as a 350 m thick basal layer beneath a resident melt. The superheated melt caused regional erosion of about 24 m thick orthocumulates at the temporary floor of the chamber by chemical dissolution, developing in addition potholes and antipotholes within the footwall rocks (shown out of scale). T - temperature.

melts (e.g., Latypov et al., 2015, 2017a, 2017c, 2020a), which is compatible with our modeling.

One aspect to consider on top of purely thermodynamic modeling, as presented here, is whether there is enough time to form regional erosional disconformities and local unconformities by chemical dissolution. The answer is most certainly 'yes', because the cooling of a melt layer in a closed system is expected to be extremely slow, approximately 0.013°C/year for a 1 km thick column of melt (Kerr, 1994), allowing the melt layer to remain superheated for centuries. It is important to note that the presented modeling is sensitive to input parameters and by increasing the degree of magma superheating we can, for example, substantially decrease the column of magma needed to melt the rocks and vice versa. What is even more important for the time scale issue is that the Bushveld chamber has been operating as an open system, with a continuous supply of new replenishing melts. Cawthorn and Walraven (1998) modelled the Bushveld chamber as a long-lived flow-through system (~75,000 years life-time) that developed via a large number of injection events, partial crystallization of these magma batches, and removal of their residual liquids from the chamber by the succeeding magma batches. They concluded that the total volume of basaltic magma involved was 740–1200 $\times$ 10^3 km^3, with only ~50% of this being represented by the cumulates now seen within the Bushveld Complex. The excess magma has likely escaped from the chamber laterally (Naldrett et al., 2012) to form mafic intrusions, such as the Molopo Farms Complex located about 200 km west of the Bushveld Complex (Prendergast, 2012; Kaavera et al., 2018).

One needs to keep in mind that the limiting factor in the dissolution process is not entirely thermodynamic, but rather kinetic and/or mechanical. Effective dissolution requires the melt residue from dissolution (i.e., a liquid boundary layer) to convect away from the surface where dissolution of floor cumulate occurs (Kerr, 1994, 1995). Convection of the contaminated melt away from the floor anorthosite contact may be possible in Case 1 – although the contaminated melts have very similar densities to those of the replenishment melt in the rhyolite-MELTS model results (Table 3), the model uncertainties leave room for convection to take place. However, during the dissolution of floor orthopyroxenite (Case 2) the contaminated melt is notably denser than the overlying pristine replenishment melt (Table 3) and it may therefore pond to the bottom and stop further dissolution. Hence the only way for dissolution to continue is if the floor was inclined so that the released melt may flow away downslope. The study by Carr et al. (1994, 1999) on the Merensky Reef potholes indicates that a temporary floor to the chamber has indeed a slope of several degrees

at the time of the formation of the Upper Critical Zone. In addition, the melt residue from dissolution can be swept away from even from the horizontal floor by the input magma, but this requires input to be continuous until dissolution is complete. In order for the chemical dissolution to take place effectively, the superheated melt must have continuous access to fresh floor cumulates, which would require effective convection in the magma body and/or assistance from some kind of mechanical removal of partly dissolved material. The destruction of the cumulates can be, perhaps, enhanced by mechanical erosion in which the dissolved material that became loose can be mobilized and physically removed by flowing magmas (e.g., Greeley et al., 1998; Williams et al., 1998). In any case, theoretical and experimental treatment of binary systems shows that chemical dissolution is expected to be most effective in large basaltic magma chambers (Kerr, 1994, 1995).

Although we are stressing here the importance of chemical dissolution, it should be noted that our thermodynamic modeling does not rule out partial melting from taking place within the floor cumulates. Rather, they just confirm that the dominant process in the formation of regionally extensive magmatic disconformities and local unconformities (i.e., potholes) must have been dissolution, not melting and that the high melting temperature of the (nearly) monomineralic cumulates is not an obstacle for their erosion as it is commonly believed. The chemical dissolution is possible and effective as far as the melts are not saturated in the liquidus phases, i.e., they do not start crystallizing from the melts. For this reason, the assimilating melts cannot be residual after fractionation of the underlying cumulates of the complex itself, but must have a distinct origin, i.e., come from outside the chamber, for instance, from a deep staging Bushveld chamber (e.g., Latypov et al., 2018, 2020a).

Finally, it should be noted that the melt that erodes the footwall rocks may be subsequently flushed away by new batches entering the chamber so that the cumulates covering the erosional surface may crystallize from the fresh melts rather than the contaminated ones (Latypov et al., 2015). If the erosion process examined in this study is a common phenomenon, then rigorous deciphering the magmatic evolution from a cumulate stratigraphy of layered intrusions may be seriously complicated by gaps caused by recharge magma cannibalization of the cumulate layers. The presented conclusions can, perhaps, be extended to other layered intrusions in which similar pothole-like erosional features have been documented (e.g., Ferguson and Pulvertatt, 1963; Halkoaho et al., 1990; Nebel et al., 2013; Boudreau, 2016).

5. Conclusions

Thermodynamic modeling using the Magma Chamber Simulator (Bohrson et al., 2014, 2020) provides some useful insights into the processes that resulted in large-scale magmatic erosion of pre-existing floor cumulates in the Bushveld Complex, South Africa. From our analysis of two spectacular occurrences of floor cumulate erosion in this plutonic body (Figs. 2-3), we can draw the following conclusions:

(1) The Bushveld chamber was growing incrementally via numerous magma replenishment events that caused, at some stratigraphic levels, magmatic erosion of, at least, 15–20 m of pre-existing floor cumulates most of which were (nearly) monomineralic in composition (anorthosites or orthopyroxenites).
(2) Thermal melting of such monomineralic cumulates is problematic because their melting temperatures are very high (1400–1500°C) so that the actual temperature of replenishing basaltic-andesitic melts (~1220–1260°C) is simply not high enough to increase the temperature of these cumulates up to their melting point.
(3) The erosion of such high-temperature-melting cumulates can, however, be accomplished via chemical dissolution by slightly superheated (15°C above the liquidus) replenishing melts that are undersaturated in the cumulus phases. The superheating may arise from the rapid ascent of a large volume of hot melt from the deep-seated reservoir with little cooling against the cold crustal rocks.
(4) Such superheated melts may enter into the chamber as basal flows along the temporary floor and can dissolve up to 4.5–8.0 wt% (relative to the mass of the melt) of the underlying cumulates of anorthositic/orthopyroxenitic composition without inducing crystallization of these melts.
(5) This mass of dissolved rocks is equivalent to regional erosion of 15–24 m of floor cumulates of anorthositic/orthopyroxenitic composition, given a basal layer of the replenishing superheated melt of about 350 m thick. The scale of erosion is sufficient to explain the relative masses of the magma and eroded cumulates in the Bushveld Complex.
(6) The regional erosion of the high-temperature-melting floor cumulates in the Bushveld chamber has thus been mostly controlled by their chemical dissolution by replenishing superheated melts. Thermal melting and mechanical disruption may also have been involved in the erosion but likely played a minor contributing role in this process.

Supplementary data

MCS model output files (Microsoft Excel files) and their summary (Microsoft Word Document) in a single zip file.

Declaration of Competing Interests

The authors declare that they have no known competing financial interests or personal relationships that could have appeared to influence the work reported in this paper.

CRediT authorship contribution statement

Rais M. Latypov: Conceptualization, Methodology, Writing – original draft. **Jussi S. Heinonen:** Methodology, Writing – review & editing. **Sofia Yu. Chistyakova:** Visualization, Writing – review & editing.

Acknowledgments

The study was supported by research grants to Rais Latypov from the NRF and DSI-NRF CIMERA of South Africa and to Jussi Heinonen from the Academy of Finland (Grant No. 295129). Any opinion, finding and conclusion expressed in this contribution is that of the authors and the NRF and DSI-NRF CIMERA do not accept any liability in this regard. We are also very grateful to Frank J. Spera, Steve Barnes and Ian Campbell for their helpful comments on an early version of the manuscript. Jussi Heinonen would specifically want to acknowledge Frank J. Spera for enlightening discussions on thermodynamics and Mikko Haaramo for standing up to defend the MCS computers from forced updates. Official reviews of the manuscript by two anonymous reviewers and editorial handling by Sohini Ganguly are gratefully acknowledged.

Supplementary materials

Supplementary material associated with this article can be found, in the online version, at doi:10.1016/j.geogeo.2022.100077.

References

Ballhaus, C.G., 1988. Potholes of the Merensky Reef at Brakspruit Shaft, Rustenburg platinum mines; primary disturbances in the magmatic stratigraphy. Econ. Geol. 83, 1140–1158. doi:10.2113/gsecongeo.83.6.1140.

Bohrson, W., Spera, F., Ghiorso, M., et al., 2014. Thermodynamic model for energy–constrained open-system evolution of crustal magma bodies undergoing simultaneous recharge, assimilation and crystallization: the magma chamber simulator. J. Petrol. 55, 1685–1717 https://doi.org/doi:10.1093/petrology/egu036.

Bohrson, W.A., Spera, F.J., Heinonen, J.S., et al., 2020. Diagnosing open-system magmatic processes using the Magma Chamber Simulator (MCS): part I—Major elements and phase equilibria. Contrib. Mineral. Petrol. 175, 104. doi:10.1007/s00410-020-01722-z.

Boudreau, A., 2019. Hydromagmatic Processes and Platinum Group Element Deposits in Layered Intrusions, 1st edn. Cambridge University Press.

Boudreau, A.E., 1992. Volatile fluid overpressure in layered intrusions and the formation of potholes. Austr. J. Earth Sci. 39, 277–287. doi:10.1080/08120099208728023.

Boudreau, A.E., 2016. The Stillwater Complex, Montana – Overview and the significance of volatiles. Mineral. Mag. 80, 585–637. doi:10.1180/minmag.2016.080.063.

Bowen, N.L., 1915. The crystallization of haplobasaltic, haplodioritic, and related magmas. Am. J. Sci. 4, 161–185.

Campbell, I.H., 1986. A fluid dynamic model for the potholes of the Merensky Reef. Econ. Geol. 81, 1118–1125. doi:10.2113/gsecongeo.81.5.1118.

Carr, H.W., Groves, D.I., Cawthorn, R.G., 1994. Controls on the distribution of Merensky Reef potholes at the Western Platinum Mine, Bushveld Complex, South Africa: implications for disruptions of the layering and pothole formation in the Complex. S. Afr. J. Geol. 97, 431–441.

Carr, H.W., Kruger, F.J., Groves, D.I., Cawthorn, R.G., 1999. The petrogenesis of Merensky Reef potholes at the Western Platinum Mine, Bushveld Complex: Sr-isotopic evidence for synmagmatic deformation. Mineral Deposita 34, 335–347. doi:10.1007/s001260050208.

Cawthorn, R.G., 2015. The Bushveld Complex, South Africa. In: Charlier, B., Namur, O., Latypov, R., Tegner, C. (Eds.), Layered Intrusions. Springer, Netherlands, Dordrecht, pp. 517–587.

Cawthorn, R.G., Walraven, F., 1998. Emplacement and crystallization time for the Bushveld Complex. J. Petrol. 39, 1669–1687.

Cheadle, M.J., Elliott, M.T., McKenzie, D., 2004. Percolation threshold and permeability of crystallizing igneous rocks: the importance of textural equilibrium. Geology 32, 757–760. doi:10.1130/G20495.1.

Chistyakova, S., Latypov, R., Hunt, E.J., Barnes, S., 2019a. Merensky-type platinum deposits and a reappraisal of magma chamber paradigms. Sci. Rep. 9, 8807. doi:10.1038/s41598-019-45288-8.

Chistyakova, S., Latypov, R., Youlton, K., 2019b. Multiple Merensky Reef of the Bushveld Complex, South Africa. Contrib. Mineral. Petrol. 174, 26. doi:10.1007/s00410-019-1562-x.

Chistyakova, S.Yu., Latypov, R.M., Kruger, F.J., Zaccarini, F., 2021. Transgressive nature and chilled margins of the Upper Zone in the western Bushveld Complex, South Africa. Can. Mineralogist 59, 1285–1303. doi:10.3749/canmin.2100027.

Eales, H.V., 2002. Caveats in defining the magmas parental to the mafic rocks of the Bushveld Complex, and the manner of their emplacement: review and commentary. Mineral. Mag. 66, 815–832. doi:10.1180/0026461026660062.

Eales, H.V., Cawthorn, R.G., 1996. The Bushveld Complex. In: Cawthorn, R.G. (Ed.), Developments in Petrology. Elsevier, pp. 181–229.

Eales, H.V., Field, M., de Klerk, W.J., Scoon, R.N., 1988. Regional trends of chemical variation and thermal erosion in the Upper Critical Zone. Western Bushveld Complex. Mineral Mag 52, 63–79. doi:10.1180/minmag.1988.052.364.06.

Ferguson, J., Pulvertatt, T.C.R., 1963. Contrasted styles of igneous layering in the Gardar Province of South Greenland. Miner. Soc. Am. Spec. Pap. 1, 10–21.

Finn, C.A., Bedrosian, P.A., Cole, J.C., et al., 2015. Mapping the 3D extent of the Northern Lobe of the Bushveld layered mafic intrusion from geophysical data. Precambrian Res. 268, 279–294. doi:10.1016/j.precamres.2015.07.003.

Gain, S.B., 1985. The geologic setting of the platiniferous UG-2 chromitite layer on the farm Maandagshoek, eastern Bushveld Complex. Econ. Geol. 80, 925–943. doi:10.2113/gsecongeo.80.4.925.

Ghiorso, M.S., Gualda, G.A.R., 2015. An H2O–CO2 mixed fluid saturation model compatible with rhyolite-MELTS. Contrib. Mineral. Petrol. 169, 53. doi:10.1007/s00410-015-1141-8.

Ghiorso, M.S., Hirschmann, M.M., Reiners, P.W., Kress, V.C., 2002. The pMELTS: a revision of MELTS for improved calculation of phase relations and major element partitioning related to partial melting of the mantle to 3GPa. Geochem. Geophys. Geosystems 3, 1–35. doi:10.1029/2001GC000217.

Greeley, R., Fagents, S.A., Harris, R.S., et al., 1998. Erosion by flowing lava: field evidence. J. Geophys. Res. 103, 27325–27345. doi:10.1029/97JB03543.

Gualda, G.A.R., Ghiorso, M.S., Lemons, R.V., Carley, T.L., 2012. Rhyolite-MELTS: a modified calibration of MELTS pptimized for silica-rich, fluid-bearing magmatic systems. J. Petrol. 53, 875–890. doi:10.1093/petrology/egr080.

Hahn, U.F., Ovendale, B., 1994. UG 2 Chromitite Layer Potholes at Wildebeestfontein North Mine, Impala Platinum Limited. J. South Afr. Inst. 3, 195–200.

Halkoaho, T.A.A., Alapieti, T.T., Lahtinen, J.J., Lerssi, J.M., 1990. The Ala-Penikka PGE reefs in the Penikat layered intrusion, Northern Finland. Mineral Petrol 42, 23–38. doi:10.1007/BF01162682.

Hasch, M., Latypov, R., 2021. Too large to be seen: regional structures in Lower and Middle group chromitites of the Bushveld Complex, South Africa. Ore Geol. Rev. 139, 104520.

Heinonen, J.S., Luttinen, A.V., Spera, F.J., Bohrson, W.A., 2019. Deep open storage and shallow closed transport system for a continental flood basalt sequence revealed with Magma Chamber Simulator. Contrib. Mineral. Petrol. 174, 87. doi:10.1007/s00410-019-1624-0.

Heinonen, J.S., Spera, F.J., Bohrson, W.A., 2021. Thermodynamic limits for assimilation of silicate crust in primitive magmas. Geology doi:10.1130/G49139.1.

Hess, H.H., 1960. Stillwater Igneous Complex, Montana: a quantitative mineralogical study. Geol. Soc. America Mem. 230.

Holness, M.B., Cawthorn, R.G., Roberts, J., 2017. The thickness of the crystal mush on the floor of the Bushveld magma chamber. Contrib. Mineral. Petrol. 172, 102. doi:10.1007/s00410-017-1423-4.

Hornsey, R.A., 2004. The geology of the UG2 chromitite layer at the Two Rivers project (Dwarsrivier 372KT, Mpumalanga), and its stratigraphic correlation within the regional setting of the Bushveld Complex. Geosci. Afr. Abstract Volume 284–285.

Hunt, E., Latypov, R., Horváth, P., 2018. The Merensky Cyclic Unit, Bushveld Complex, South Africa: Reality or Myth? Minerals 8, 144. doi:10.3390/min8040144.

Iacono-Marziano, G., Ferraina, C., Gaillard, F., et al., 2017. Assimilation of sulfate and carbonaceous rocks: experimental study, thermodynamic modeling and application to the Noril'sk-Talnakh region (Russia). Ore Geol. Rev. 90, 399–413. doi:10.1016/j.oregeorev.2017.04.027.

Irvine, T.N., JCØ, Andersen, Brooks, C.K., 1998. Included blocks (and blocks within blocks) in the Skaergaard intrusion: geologic relations and the origins of rhythmic modally graded layers. Geol. Soc. Am. Bull. 110, 1398–1447.

Irvine, T.N., Keith, D.W., Todd, S.G., 1983. The J-M Platinum-Palladium Reef of the Stillwater Complex, Montana: II. origin by double-diffusive convective magma mixing and implications for the Bushveld Complex. Econ. Geol. 78, 1287–1334.

Kaavera, J., Rajesh, H.M., Tsunogae, T., Belyanin, G.A., 2018. Marginal facies and compositional equivalents of Bushveld parental sills from the Molopo Farms Complex layered intrusion, Botswana: petrogenetic and mineralization implications. Ore Geol. Rev. 92, 506–528. doi:10.1016/j.oregeorev.2017.12.001.

Kerr, R.C., 1995. Convective crystal dissolution. Contrib. Mineral. Petrol. 121, 237–246. doi:10.1007/BF02688239.

Kerr, R.C., 1994. Dissolving driven by vigorous compositional convection. J. Fluid Mech. 280, 287–302. doi:10.1017/S0022112094002934.

Kruger, F.J., 2005. Filling the Bushveld Complex magma chamber: lateral expansion, roof and floor interaction, magmatic unconformities, and the formation of giant chromitite, PGE and Ti-V-magnetitite deposits. Mineral Deposita 40, 451–472. doi:10.1007/s00126-005-0016-8.

Kruger, W., Latypov, R., 2020. Fossilized solidification fronts in the Bushveld Complex argue for liquid-dominated magmatic systems. Nat. Commun. 11, 2909. doi:10.1038/s41467-020-16723-6.

Kruger, W., Latypov, R., 2021. Magmatic karst reveals dynamics of crystallization and differentiation in basaltic magma chambers. Sci. Rep. 11, 7341. doi:10.1038/s41598-021-86724-y.

Latypov, R., Chistyakova, S., Barnes, S.J., et al., 2022. Chromitite layers indicate the existence of large, long-lived, and entirely molten magma chambers. Sci. Rep. 12, 4092. doi:10.1038/s41598-022-08110-6.

Latypov, R., Chistyakova, S., Costin, G., et al., 2020a. Monomineralic anorthosites in layered intrusions are indicators of the magma chamber replenishment by plagioclase-only-saturated melts. Sci. Rep. 10, 3839. doi:10.1038/s41598-020-60778-w.

Latypov, R., Chistyakova, S., Kramers, J., 2018a. Reply to Discussion of "Arguments against synmagmatic sills in the Bushveld Complex, South Africa" by Roger Scoon and Andrew Mitchell (2018). S. Afr. J. Geol. 121, 211–216. doi:10.25131/sajg.121.0014.

Latypov, R., Chistyakova, S., Kramers, J.D., 2017a. Arguments against syn-magmatic sills in the Bushveld Complex, South Africa. S. Afr. J. Geol. 120 (4), 565–574. doi:10.25131/gssajg.120.4.565.

Latypov, R., Chistyakova, S., Merwe, J.van derV.D., Westraat, J., 2019. A note on the erosive nature of potholes in the Bushveld Complex. S. Afr. J. Geol. 122, 555–560. doi:10.25131/sajg.122.0042.

Latypov, R., Chistyakova, S., Mukherjee, R., 2017b. A novel hypothesis for origin of massive chromitites in the Bushveld Igneous Complex. J. Petrol. 58, 1899–1940. doi:10.1093/petrology/egx077.

Latypov, R., Chistyakova, S., Page, A., Hornsey, R., 2015. Field evidence for the in situ crystallization of the Merensky Reef. J. Petrol. 56, 2341–2372. doi:10.1093/petrology/egv023.

Latypov, R., Costin, G., Chistyakova, S., et al., 2018b. Platinum-bearing chromite layers are caused by pressure reduction during magma ascent. Nat. Commun. 9. doi:10.1038/s41467-017-02773-w.

Latypov, R.M., Chistyakova, S. Yu, Barnes, S.J., Hunt, E.J., 2017c. Origin of platinum deposits in layered intrusions by in situ crystallization: evidence from undercutting Merensky Reef of the Bushveld Complex. J. Petrol. 58, 715–762. doi:10.1093/petrology/egx032.

Latypov, R.M., Chistyakova, S.Yu., Namur, O., Barnes, S., 2020b. Dynamics of evolving magma chambers: textural and chemical evolution of cumulates at the arrival of new liquidus phases. Earth Sci. Rev. 210, 103388. doi:10.1016/j.earscirev.2020.103388.

Leeb-Du Toit, A., 1986. The Impala Platinum Mines. In: Anhaeusser, C.R., Maske, S. (Eds.), Mineral Deposits of Southern Africa. Mineral deposits of Southern Africa. Geological Society of South Africa, pp. 1091–1106.

Lomberg, K.G., Patterson, M.A., Venter, J.E., Martin, E.S., 1999. The morphology of potholes in the UG2 chromitite layer and Merensky Reef (pothole reef facies) at Union Section, Rustenberg Platinum Mines. S. Afr. J. Geol. 102, 209–220.

Maier, W.D., Barnes, S.-J., Groves, D.I., 2013. The Bushveld Complex, South Africa: formation of platinum–palladium, chrome- and vanadium-rich layers via hydrodynamic sorting of a mobilized cumulate slurry in a large, relatively slowly cooling, subsiding magma chamber. Mineral Deposita 48, 1–56. doi:10.1007/s00126-012-0436-1.

Maier, W.D., Karykowski, B.T., Yang, S.-.H., 2016. Formation of transgressive anorthosite seams in the Bushveld Complex via tectonically induced mobilisation of plagioclase-rich crystal mushes. Geosci. Front. doi:10.1016/j.gsf.2016.06.005.

Marsh, B.D., 1996. Solidification fronts and magmatic evolution. Mineral. Mag. 60, 5–40.

Marsh, B.D., 2006. Dynamics of magmatic systems. Elements 2, 287–292. doi:10.2113/gselements.2.5.287.

Marsh, B.D., 2013. On some fundamentals of igneous petrology. Contrib. Mineral. Petrol. 166, 665–690. doi:10.1007/s00410-013-0892-3.

Mitchell, A.A., Henckel, J., Mason-Apps, A., 2019a. The Upper Critical Zone of the Rustenburg Layered Suite in the Swartklip Sector, north-western Bushveld Complex, on the farm Wilgerspruit 2JQ: I. Stratigraphy and PGE mineralization patterns. S. Afr. J. Geol. 122, 117–142. doi:10.25131/sajg.122.0010.

Mitchell, A.A., Scoon, R.N., Sharpe, M.R., 2019b. The Upper Critical Zone in the Swartklip Sector, north-western Bushveld Complex, on the farm Wilgerspruit 2JQ: II. Origin by intrusion of ultramafic sills with concomitant partial melting of host norite-anorthosite cumulates. S. Afr. J. Geol. 122, 143–162. doi:10.25131/sajg.122.0011.

Morse, S.A., 1980. Basalts and Phase diagrams: an Introduction to the Quantitative Use of Phase Diagrams in Igneous Petrology. Springer-Verlag.

Mukherjee, R., Latypov, R., Balakrishna, A., 2017. An intrusive origin of some UG-1 chromitite layers in the Bushveld Igneous Complex, South Africa: insights from field relationships. Ore Geol. Rev. 90, 94–109. doi:10.1016/j.oregeorev.2017.03.008.

Müller, A., Breiter, K., Seltmann, R., Pécskay, Z., 2005. Quartz and feldspar zoning in the eastern Erzgebirge volcano-plutonic complex (Germany, Czech Republic): evidence of multiple magma mixing. Lithos 80, 201–227. doi:10.1016/j.lithos.2004.05.011.

Mungall, J.E., 2007. Crustal contamination of picritic magmas during transport through dikes: the Expo Intrusive Suite, Cape Smith Fold Belt, New Quebec. J. Petrol. 48, 1021–1039. doi:10.1093/petrology/egm009.

Naldrett, A.J., Wilson, A., Kinnaird, J., et al., 2012. The origin of chromitites and related PGE mineralization in the Bushveld Complex: new mineralogical and petrological constraints. Mineral Deposita 47, 209–232. doi:10.1007/s00126-011-0366-3.

Nebel, O., Arculus, R.J., Ivanic, T.J., et al., 2013. Upper Zone of the Archean Windimurra layered mafic intrusion, Western Australia: insights into fractional crystallisation in a large magma chamber. N. Jb. Miner. Abh. 191, 83–107. doi:10.1127/0077-7757/2013/0249.

Pebane, M., Latypov, R., 2017. The significance of magmatic erosion for bifurcation of UG1 chromitite layers in the Bushveld Complex. Ore Geol. Rev. 90, 65–93. doi:10.1016/j.oregeorev.2017.02.026.

Prendergast, M.D., 2012. The Molopo Farms Complex, southern Botswana - a reconsideration of structure, evolution, and the Bushveld connection. S. Afr. J. Geol. 115, 77–90. doi:10.2113/gssajg.115.1.77.

Presnall, D.C., Dixon, S.A., Dixon, J.R., et al., 1978. Liquidus phase relations on the join diopside-forsterite-anorthite from 1 atm to 20 kbar: their bearing on the generation and crystallization of basaltic magma. Contrib. Mineral. Petrol. 66, 203–220. doi:10.1007/BF00372159.

Roberts, M.D., Reid, D.L., Miller, J.A., et al., 2007. The Merensky Cyclic Unit and its impact on footwall cumulates below Normal and Regional Pothole reef types in the. Western Bushveld Complex. Mineral Deposita 42, 271–292. doi:10.1007/s00126-006-0111-5.

Robie, R.A., Waldbaum, D.R., 1968. Thermodynamic properties of minerals and related substances at 298.15K (25.0 C) and one atmosphere (1.013 bars) pressure and at higher temperatures. Bull. US Geol. Surv. 1259, 256.

Schmidt, E.R., 1952. The structure and composition of the Merensky reef and associated rocks on the Rustenburg platinum mine. S. Afr. J. Geol. 55, 233–279.

Smith, D.S., Basson, I.J., 2006. Shape and distribution analysis of Merensky Reef potholing, Northam Platinum Mine, western Bushveld Complex: implications for pothole formation and growth. Mineral Deposita 41, 281–295. doi:10.1007/s00126-006-0059-5.

Smith, D.S., Basson, I.J., Reid, D.L., 2004. Normal reef subfacies of the Merensky Reef at Northam platinum mine, Zwartklip facies, Western Bushveld Complex, South Africa. Can. Mineral. 42, 243–260. doi:10.2113/gscanmin.42.2.243.

Spera, F.J., Schmidt, J.S., Bohrson, W.A., Brown, G.A., 2016. Dynamics and thermodynamics of magma mixing: insights from a simple exploratory model. Am. Mineral. 101, 627–643. doi:10.2138/am-2016-5305.

Van der Merwe, J., Cawthorn, R.G., 2005. Structures at the base of the Upper Group 2 chromitite layer, Bushveld Complex, South Africa, on Karee Mine (Lonmin Platinum). Lithos 83, 214–228. doi:10.1016/j.lithos.2005.03.003.

Viljoen, M.J., 1999. The nature and origin of the Merensky Reef of the western Bushveld Complex based on geological facies and geological data. S. Afr. J. Geol. 102, 221–239.

Viljoen, M.J., Hieber, R., 1986. The Rustenburg section of Rustenburg Platinum Mines Limited, with reference to the Merensky Reef. In: Anhaeusser, C.R., Maske, S. (Eds.), Mineral Deposits of Southern Africa. Mineral deposits of Southern Africa. Geological Society of South Africa, pp. 1117–1134.

Viljoen, M.J., Klerk, WJ de, Coertze, P.M., et al., 1986. The Union section of Rustenburg Platinum Mines Limited, with reference to the Merensky Reef. In: Anhaeusser, C.R., Maske, S. (Eds.), Mineral Deposits of Southern Africa. Mineral deposits of Southern Africa. Geological Society of South Africa, pp. 1061–1090.

Viring, R.G., Cowell, M.W., 1999. The Merensky Reef on Northam Platinum Limited. S. Afr. J. Geol. 102 (3), 192–208.

Willemse, J., 1959. The “floor” of the Bushveld Igneous Complex and its relationships, with special reference to the Eastern Transvaal. S. Afr. J. Geol. 62, 21–83.

Williams, D.A., Kerr, R.C., Lesher, C.M., 1998. Emplacement and erosion by Archean komatiite lava flows at Kambalda: revisited. J. Geophys. Res. 103, 27533–27549. doi:10.1029/97JB03538.

Yoder, H.S., 1976. Generation of Basaltic Magma. National Academy of Sciences, Washington, DC.